Simultaneous Magnetic Resonance Angiography and Multiparametric Mapping in the Transient-state

Pedro A. Gómez[1,2], Miguel Molina-Romero[1,2], Guido Buonincontri[3], Bjoern H. Menze[1], Marion I. Menzel[1,2]

[1]Computer Science, Technische Universität München, Munich, Germany
[2]GE Healthcare, Munich, Germany
[3]IMAGO7 Foundation, Pisa, Italy

Abstract. Quantitative Transient-state Imaging (QTI) is a non-random, dictionary-less MR Fingerprinting alternative. Through iterative reconstructions, QTI recovers a series of contrast-weighted images from transient-state acquisitions and subsequently estimates the parameters that best describe the resulting dynamic signal evolutions. Here, we extend the QTI framework by incorporating a simple velocity model that accounts for blood flowing into and out of the imaging slice. The model, however wrong, can be very useful: it predicts signal hyperintensities in the presence of flow, allowing for the simultaneous reconstruction of MR Angiography images, hundreds of dynamic contrast-weighted images, and their corresponding parametric maps.

1 Introduction

Multiparametric mapping methods, such as Quantitative Transient-state Imaging [4] and MR Fingerprinting [6], enable the estimation of several parametric maps with a single acquisition by enforcing consistency with a model. If such model is assumed to be perfect, the estimated parametric maps contain all the relevant information. However, commonly used models have limitations, and by consequence the maps can disregard useful information.

This work proposes to simultaneously reconstruct images and compute parametric maps, and demonstrates that simple models, however wrong, can be very useful in the context of contrast-weighted imaging. For example, by accounting for blood flowing through an imaging slice with a mean velocity scalar, it is possible to predict a signal hyperintensity throughout the course of the acquisition. Thus, the reconstructed signals can be taken advantage of to obtain MR Angiography (MRA) images. In the following, we clarify how to incorporate flow into transient-state acquisitions and show results for simultaneous MRA, contrast-weighted imaging, and multiparametric mapping in the transient-state.

2 Methods

In the transient-state, the observed signal over time $y(t) \in \mathbb{C}^T$ with T measurements can be described as a spatial function modulated by a temporal signal:

$$y(t) = \int_{\mathbf{r}} \rho(\mathbf{r}) f_t(\mathbf{r}) e^{-2\pi i \mathbf{k}(t)\cdot\mathbf{r}} d\mathbf{r}; \tag{1}$$

where $\rho(\mathbf{r})$ is the spin density at position $\mathbf{r}$, $\mathbf{k}(t)$ is the k-space trajectory, and $f_t(\mathbf{r})$ is the temporal signal, given by the recursion:

$$f_t(\mathbf{r}) = \sum_{i=0}^{T} f_{t-1}(\mathbf{r}) g\left(\eta_i; \theta(\mathbf{r})\right) * h_i(t). \tag{2}$$

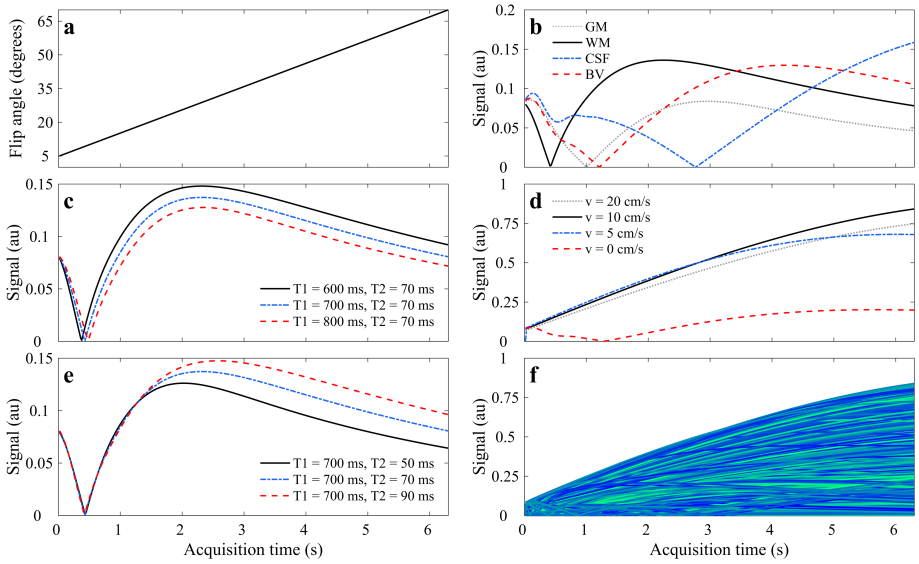

Fig. 1. Plug flow and washout from an imaging slice. a, Fraction of spins $h(t)$ remaining in a slice after being tagged by an RF pulse at $h(0)$, where d is the slice thickness and v is the mean velocity. **b-d**, The total number of repetitions that spins tagged by a certain pulse remain in the slice is proportional to their velocity, where spins flowing slowly will remain in the slice longer than faster spins. Furthermore, the starting fraction of fresh spins in a subsequent RF pulse is equivalent to the fraction of spins that have washed out from the previous pulse.

The signal $f_t(\mathbf{r})$ is determined at sample time i by an operation $g(\cdot)$ on the signal from the previous sample $f_{t-1}(\mathbf{r})$, where the operator $g(\cdot)$ is a function of two parameter sets: the temporally varying acquisition parameters η_i, and the spatially dependent biophysical parameters of interest, such as $T_1(\mathbf{r})$ and $T_2(\mathbf{r})$.

Finally, $h_i(t)$ gives the fraction of spins tagged with RF pulse i that will remain in the imaging slice after time t. We have chosen $h(t)$ as plug flow (Fig. 1, that is, a constant velocity scalar over time [1]. When there is no flow, i.e. $h_i(t) = 1$, tissues become saturated and follow the dynamics dictated by η_i. With flow, fresh magnetization predicts signal hyperintensities throughout the acquisition (Fig. 2).

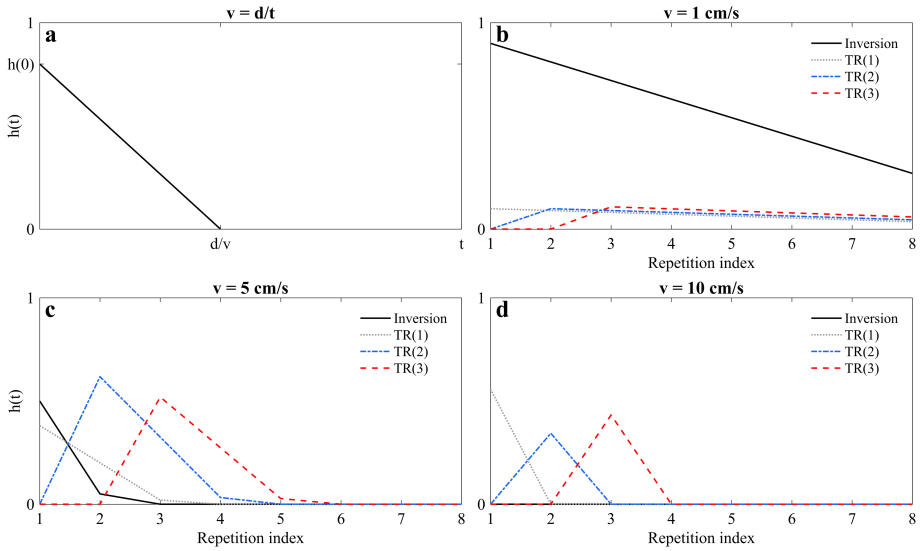

Fig. 2. Acquisition scheme and signal modeling. a, Flip angle trajectory, where an inversion pulse followed by a linear flip angle ramp provides T_1 encoding **(c)** at different inversion times and T_2 encoding from stimulated echoes at higher flip angles **(e)**. **b**, Signal evolution for four distinct tissue classes, gray matter (GM), white matter (WM), cerebrospinal fluid (CSF), and stationary blood (BV). **d**, In the presence of flow, there will be unsaturated magnetization in every repetition, producing signal hyperintensities. **f**, An ensemble of simulated stationary and flowing signal evolutions can be taken advantage of to recover the temporal signal dynamics for every voxel in the image.

We acquired 112, 2 mm thick slices of a healthy volunteer on a GE 3T MR750w scanner with a 12 channel receive only head RF coil (GE Medical Systems, Milwaukee, WI). For every slice, we inverted the magnetization locally and then applied a train of T=260 RF pulses with a flip angle ramp from 7 to 70 degrees, and TR/TE=14/2 ms. In every repetition, we acquired data with a variable density spiral with 1.3 mm in-plane resolution and reconstructed the entire four-dimensional dataset using the reconstruction proposed in [4], where we projected the data onto a lower dimensional temporal subspace [10] and regularized the reconstruction with a local low-rank operation on 4D spatiotemporal image patches. We created the subspace by sampling a prior distribution of tis-

sue classes for both stationary and non-stationary tissues (Fig. 3 and Fig. 2f) and simulated the signal over time using the Extended Phase Graph formalism [11]. After reconstruction, we estimated T_1, T_2 and proton density (PD) from the temporal dynamics and summed all temporal frames into one volume to create MRA images.

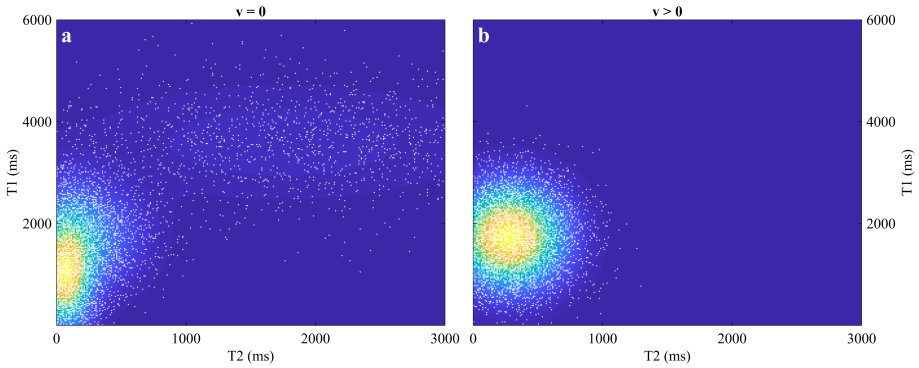

Fig. 3. Prior sampling. **a**, Four stationary tissue classes (WM, GM, CSF, and BV) were considered, where the ranges of each tissue class were informed from literature [5,2,3,7,9,9,8]. We used the following T_1/T_2 ranges: WM 661-1155/52-72 ms; GM 945-1934/61-106 ms; CSF 3200-400/1000-2500; BV 1465-2020/225-325. **b**, In the non-stationary case, only the BV prior was taken into account. Velocity was sampled evenly from 0 cm/s to 100 cm/s, which is the upper bound for spins remaining in the slice with an echo time of 2 ms and a slice thickness of 2 mm.

3 Results

Figure 4 shows several slices of the obtained MRA images, contrast-weighted images at different points in time, and their resultant parametric maps. The MRA images give anatomical context of the location of veins and arteries inside and around the brain. The contrast-weighted images provide unique contrasts and are informative on the T_1 and T_2 times of different tissues. For example, at $t = 378$ ms, white matter is close to its inversion time, whereas gray matter has not yet inverted; at $t = 684$ ms, contrast is reversed as gray matter reaches its inversion while white matter recovers signal and is still not affected by T_2 relaxation. The estimated parametric maps are consistent with previous literature findings [5,2,3,7,9,9,8]. Figure 5 displays a maximum intensity projection of the MRA images, where important structures such as the circle of Willis, the carotid arteries, and the superior sagittal sinus can be identified. Pulsatile artifacts on the slices, especially in the neck region, can also be observed.

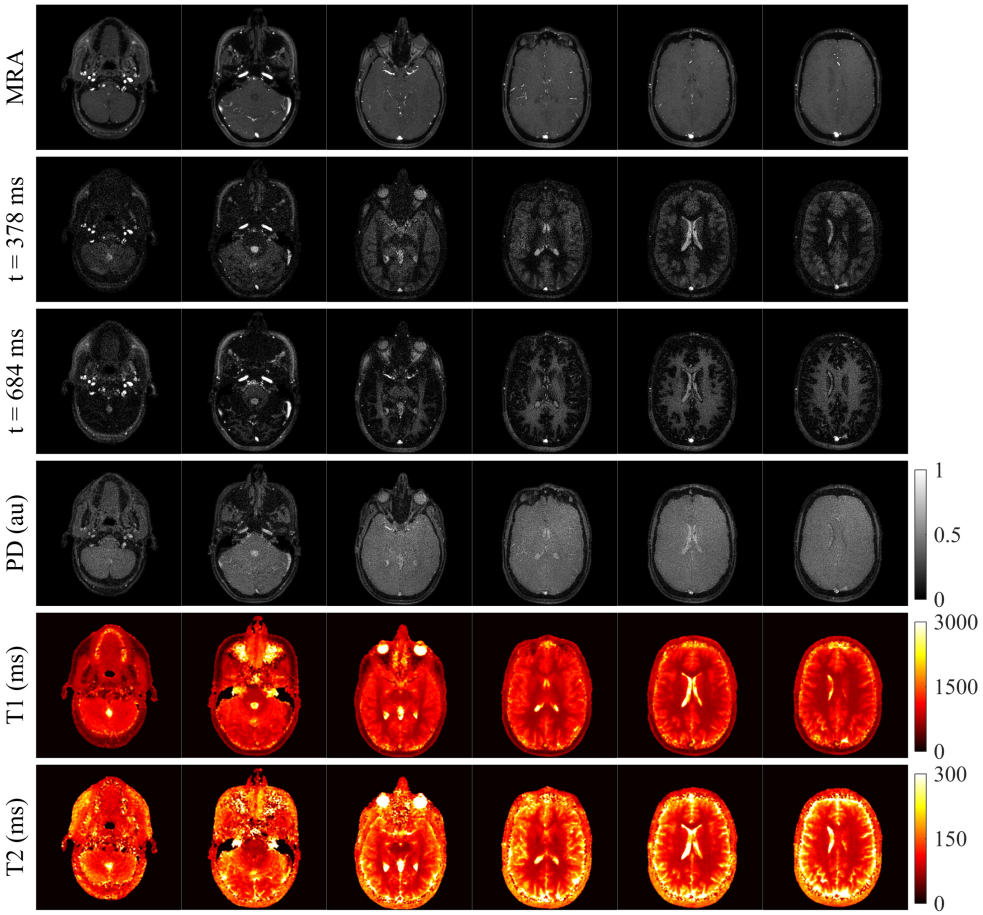

Fig. 4. Simultaneous MRA, contrast-weighted imaging, and parametric mapping. Accounting for flow effects allows for the simultaneous reconstruction of MRA images, as many contrast-weighted images as repetitions in the sequence, and the related parametric maps.

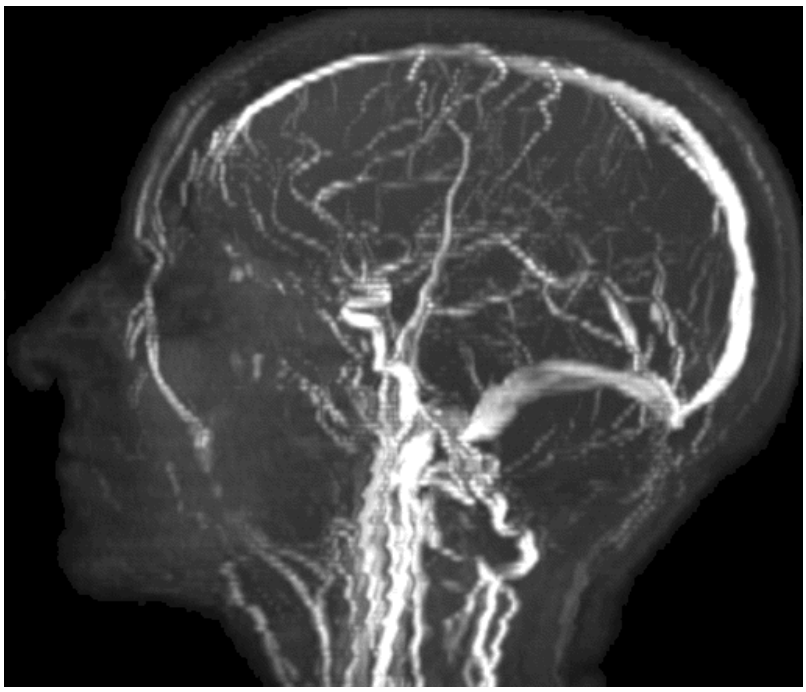

Fig. 5. 3D maximum intensity projection of MRA data. The MRA volume was obtained by summing all of the frames in the transient-state acquisition. Thereafter, a 3D maximum intensity projection results in the visualization of all of the main vascular structures in the head.

4 Discussion

By acquiring thin axial slices, we were able to make use of time-of-flight effects in the transient-state to recover MRA images. While our model relies on a velocity scalar that oversimplifies the complex reality of blood flow inside vessels, it still enables us to create MRA images that could have significant diagnostic value.

5 Conclusion

We demonstrated an extension to QTI that allows for the reconstruction of MRA images, multiple contrast-weighted images, and parametric maps from the same scan.

Acknowledgments

With the support of the TUM Institute for Advanced Study, funded by the German Excellence Initiative and the European Commission under Grant Agreement Number 605162.

References

1. Axel, L.: Blood flow effects in magnetic resonance imaging. Am.J.Roentgeno. 143, 1157–1166 (1984)
2. Ethofer, T., Mader, I., Seeger, U., Helms, G., Erb, M., Grodd, W., Ludolph, A., Klose, U.: Comparison of Longitudinal Metabolite Relaxation Times in Different Regions of the Human Brain at 1.5 and 3 Tesla. Magnetic Resonance in Medicine 50(6), 1296–1301 (2003)
3. Gelman, N., Gorell, J.M., Barker, P.B., Savage, R.M., Spickler, E.M., Windham, J.P., Knight, R.A.: MR Imaging of Human Brain at 3.0 T: Preliminary Report on Transverse Relaxation Rates and Relation to Estimated Iron Content. Radiology 210(3), 759–767 (1999)
4. Gómez, P.A., Buonincontri, G., Molina-Romero, M., Sperl, J.I., Menzel, M.I., Menze, B.H.: Accelerated parameter mapping with compressed sensing: an alternative to MR Fingerprinting. Proc Intl Soc Mag Reson Med (2017)
5. Lu, H., Nagae-Poetscher, L.M., Golay, X., Lin, D., Pomper, M., Van Zijl, P.C.M.: Routine clinical brain MRI sequences for use at 3.0 tesla. Journal of Magnetic Resonance Imaging 22(1), 13–22 (2005)
6. Ma, D., Gulani, V., Seiberlich, N., Liu, K., Sunshine, J.L., Duerk, J.L., Griswold, M.A.: Magnetic resonance fingerprinting. Nature 495, 187–192 (2013)
7. MacKay, A., Laule, C., Vavasour, I., Bjarnason, T., Kolind, S., Mädler, B.: Insights into brain microstructure from the T2 distribution. Magnetic Resonance Imaging 24(4), 515–525 (2006)
8. Noeske, R., Seifert, F., Rhein, K.H., Rinneberg, H.: Human cardiac imaging at 3 T using phased array coils (2000), http://doi.wiley.com/10.1002/1522-2594{%}28200012{%}2944{%}3A6{%}3C978{%}3A{%}3AAID-MRM22{%}3E3.0.CO{%}3B2-9

9. Smith, S.A., Edden, R.A.E., Farrell, J.A.D., Barker, P.B., Van Zijl, P.C.M.: Measurement of T1 and T2 in the cervical spinal cord at 3 Tesla. Magnetic Resonance in Medicine 60(1), 213–219 (2008)
10. Tamir, J.I., Uecker, M., Chen, W., Lai, P., Alley, M.T., Vasanawala, S.S., Lustig, M.: T2 shuffling: Sharp, multicontrast, volumetric fast spin-echo imaging. Magnetic Resonance in Medicine (2016)
11. Weigel, M.: Extended phase graphs: Dephasing, RF pulses, and echoes - pure and simple. Journal of Magnetic Resonance Imaging (2014)